Res Chem Intermed
DOI 10.1007/s11164-017-3089-y

Synthesis, characterization, biological screening and molecular docking studies of 2-aminonicotinaldehyde (ANA) and its metal complexes

Ramaiah Konakanchi[1] · Ramachary Mallela[2] · Ramu Guda[3] · Laxma Reddy Kotha[1]

Received: 25 April 2017 / Accepted: 21 July 2017

Abstract The biological and optical importance of the o-aminoaldehyde family of ligands inspired us to evaluate the coordination properties and biological activities of 2-aminonicotinaldehyde (ANA). Here, we report the synthesis, characterization, biological screening and molecular docking studies of ANA and its metal complexes of Ni(II), Pd(II), Co(II) and Cu(II) using various analytical and spectroscopic techniques. The single crystal X-ray diffraction studies of ANA explain the solid-state assembly and an interesting supramolecular herring bone stacking pattern by classical N–H···O/N intra/inter molecular and non-classical C–H···O/N intermolecular H-bonding. ANA and its metal complexes were screened for in vitro anticancer, antimicrobial and anti-oxidant activities. Anticancer activity was tested against HeLa, MCF-7 and HEK293 human cancer cell lines. The $[Ni(ANA)_2Cl_2]$ complex showed good activity against HeLa and MCF-7, the $[Pd(ANA)_2Cl_2]$ and $[Cu(ANA)_2Cl_2]$ complexes against HeLa, and the $[Co(ANA)_2Cl_2]$ complex against MCF-7. In antimicrobial screening, the $[Co(ANA)_2Cl_2]$ and $[Cu(ANA)_2Cl_2]$ complexes were proved to be potent antibacterial and antifungal agents. The anti-oxidant activity of these complexes was investigated through DPPH radical assay, and it was found that all the complexes have good radical scavenging capability. Molecular docking studies were also carried for all the metal complexes against EGFR as a target protein by using Autodock, and the results strongly correlated with the anticancer activity.

✉ Laxma Reddy Kotha
laxmareddychem12@gmail.com

[1] Department of Chemistry, National Institute of Technology, Warangal 506004, India

[2] Department of Chemistry, Lal Bahadur College, Warangal 506007, India

[3] Department of Chemistry, Kakatiya University, Warangal 506009, India

Published online: 07 August 2017

Keywords Metal complexes · 3D architecture · Antimicrobial activity · Anticancer activity · Anti-oxidant activity · Docking studies

Introduction

In recent years, modern coordination chemistry has expanded its horizons to emerging areas of metal organic frameworks [1–4], crystal engineering [5], nonlinear optical materials [6–10] and other areas of interdisciplinary research. Several classes of ligand architectures have been developed over the years to suit appropriate applications. One such class of ligands with scarce literature citations are the o-aminoaldehydes. Historically, o-aminoaldehydes have often been employed as important building blocks for several pharmaceutically relevant compounds like naphthyridine derivatives (for osteoporosis) [11], plant-antitumor agents (camptothecin analogues) [12], antihistamine and pain-relieving agents (mGlu5 receptor antagonist) [13] (Fig. 1). The reaction of pyridine in o-aminobenzaldehyde (2-aminonicotinaldehyde, ANA) with cyclic aliphatic diketones (1,3-diketocyclohexane) yields fused polypyridyl compounds which have been extensively used to prepare polymetallic complexes having interesting magnetic properties [14] (Schemes 1). The metal binding affinities of o-aminoaldehydes have not been extensively studied. Eichhorn and co-workers have reported the Cu(II) complexes of o-aminobenzaldehyde. Preliminary spectral characterization revealed a di-copper complex [15]. The coordination chemistry of ANA was quite different from that of the parent ligand. Theoretically, there are three plausible metal binding sites in ANA, pyridine N being the probable electron donor site, others include the amine N and the aldehyde O as is the case with o-aminobenzaldehyde. Usually, ancillary ligands have been employed along with ANA to satisfy the coordination number of the metal. In all cases, pyridine N was found to be binding to the metal center.

A detailed literature search on the coordination chemistry of ANA (without ancillary ligands) did not produce any results. The only comparable complexes reported were the Zn(II) complexes of 2-aminopyridine and 3-pyridinealdehyde [16, 17]. These complexes were reported to show excellent non-linear optical properties (Fig. 2). The structure of ANA is shown in Fig. 3. The option of having more than one potential metal binding site makes the investigation of the coordination chemistry of ANA very challenging. Equipped with the knowledge on

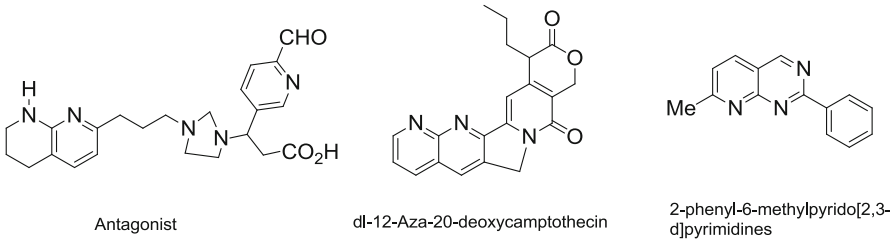

Antagonist

dl-12-Aza-20-deoxycamptothecin

2-phenyl-6-methylpyrido[2,3-d]pyrimidines

Fig. 1 Application of o-aminoaldehlydes as synthetic building blocks for pharmaceutical applications

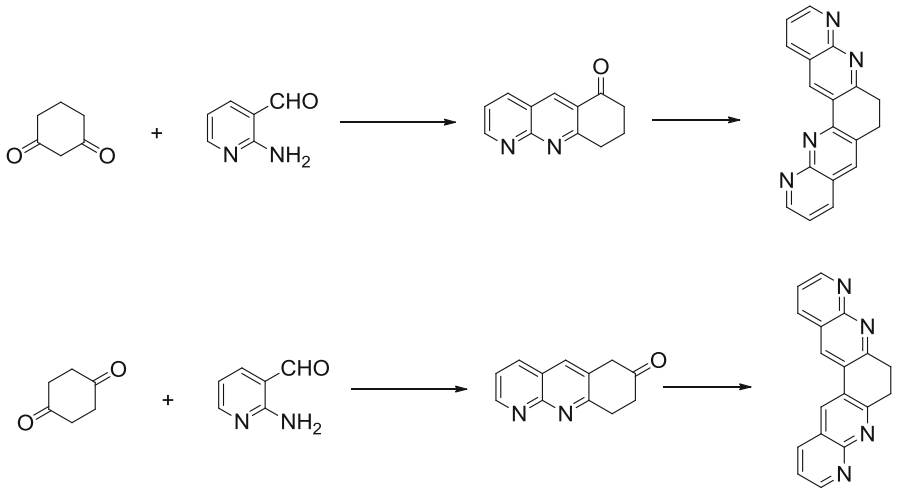

Scheme 1 Application of o-aminoaldehydes for the synthesis of fused polypyridyl ligands

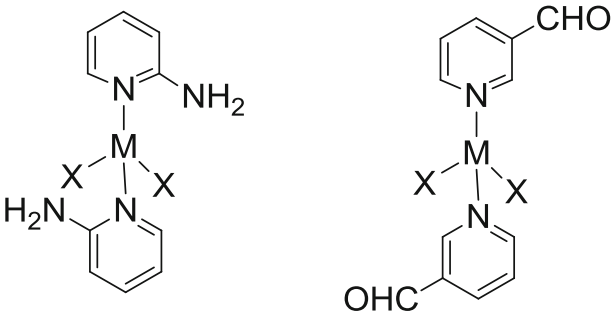

Fig. 2 M = Zn(II) complexes of 2-aminopyridine and 3-pyridinaldehyde

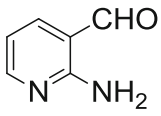

Fig. 3 Structure of 2-aminonicotinaldehyde (ANA)

the biological and optical importance of amino and aldehyde of pyridine analogues, we set out to explore the coordination properties of ANA with metals like Ni(II), Pd(II), Co(II) and Cu(II). Different analytical tools, UV–Vis, FTIR, docking studies

and cyclic voltamograms, were employed to understand the metal binding affinity of ANA in the metal complexes.

Experimental

General information

All reactions were performed using dry solvents and standard Schlenk techniques. The ligand ANA was prepared as reported previously [18]. Nicotinamide and ammonium sulfamate were purchased from Loba Chemie, and nickel(II) chloride hexahydrate, palladium(II) chloride, copper(II) chloride, cobalt(II) chloride hexahydrate and CDCl3 (99.9% D, containing 0.03% TMS) were purchased from Aldrich (USA). Iron(II) triflate diacetonitrile was prepared according to known procedures [19]. The drying agents employed at various stages of purification procedures, i.e., anhydrous sodium sulfate, calcium hydride and sodium hydroxide and hydrochloric acid of analytical reagent grade were obtained from Ranbaxy (India). The nitrogen gas utilized in this study was obtained from Jainex Gases (India). It was further purified by using a P_2O_5/KOH tower, and molecular sieves, methanol and acetonitrile were of spectroscopic grade from Merck (India). They were further purified by distilling over calcium hydride [20, 21].

Materials, methods and equipment

All the compounds synthesized during this study were characterized by recording their melting point, nuclear magnetic resonance (^{1}H and ^{13}C), infrared and electronic absorption spectra and by electrochemical (cyclic-voltammetry) methods and docking studies. Melting points were measured by using Bucchi–Electrothermal melting point apparatus and elemental analysis by using a Vario MICRO CHNS/15082029 analyzer. The ^{1}H NMR and ^{13}C NMR spectra were recorded on a Bruker Ascend-400 MHz spectrometer using DMSO-d_6 as the solvent at ambient temperatures. Tetramethylsilane (TMS) was the internal standard employed while recording these spectra. IR spectra were recorded on a Perkin-Elmer 100S spectrophotometer by dispersing the solid samples with KBr pellets. The electronic spectra of the ligands and their metal complexes were recorded on a Hewlett-Packard 8452 diode-array spectrometer equipped with HP-chemstation software. Cyclic-and differential-pulse voltammetric experiments (CH_3CN, 0.1 M TBAP) were performed on a CH Instruments model CHI 620A electrochemical analyzer (working and auxiliary electrodes: Pt; reference electrode: Ag/AgCl). A Fc^+/Fc (Fc = ferrocene) couple was used to calibrate the redox potential values.

Crystal structure determination

A single crystal of the ligand ANA suitable for X-ray diffraction analysis was obtained by slow evaporation from ethanol solution. The diffraction data were collected on a Bruker SMART APEX-II CCD diffractometer, equipped with a fine

focus 1.75-Kw sealed tube Mo-kα radiation (λ = 0.71073 Å) at 296 K, with increasing omega width of 0.3° per frame at a scan speed of 5 s/frame. Data integration and reduction were carried out with the help of the SAINT program [22]. Multiscan empirical absorption corrections were applied to the data using the program SADABS [23]. Structures were solved by direct methods and refined with full-matrix least squares on F^2 using the SHELXL–97 program [24]. All non-hydrogen atoms were refined anisotropically. The hydrogen atoms were located from the Fourier maps and refined. Structural illustrations have been drawn with Cameron and ORTEP software.

Synthesis

Synthesis of 2-aminonicotinaldehyde

The ligand ANA was prepared as per the procedure reported in the literature [18] and, on recrystallization from ethanol,yielded yellow crystals suitable for X-ray diffraction. Yield 40%. Anal. Calcd. For $C_6H_6N_2O$ (%): C, 58.95; H, 4.91; N, 22.93. Found: C, 58.80; H, 4.80; N, 22.87. M.P 99 °C; IR (KBr, cm^{-1}): 3396 [$_{(N–H)}$], 1667 [$\upsilon_{(c=0)}$], 1575 [$\upsilon_{(c=N)\ (Py)}$]. ^{1}HNMR (DMSO, ppm, 400 MHz): δ 9.84 (s, 1H), 8.24 (d, J = 8.0 Hz, 1H), 8.00 (d, J = 8.0 Hz, 1H), 7.55 (s, 2H, –NH_2), 6.72–6.75 (m, 1H). ^{13}CNMR (DMSO, ppm, 100 MHz): δ 194.12, 158.70, 155.36, 145.02, 113.44, 112.69.

Nickel(II) complex of 2-aminonicotinaldehyde

This complex was prepared by direct reaction between the freshly purified ligand (0.244 g, 2 mmol) and nickel(II) chloride hexahydrate $NiCl_2{\cdot}6H_2O$ (0.2376 g, 1 mmol). It was dissolved in 50 mL of anhydrous methanol and refluxed for 3–4 h. The color of the reaction mixture changed from pale yellow to reddish brown. At the end of the reaction, a reddish brown solid was obtained which was recrystallized from methanol to obtain 75% yield. Anal. Calcd. for [$Ni(C_6H_6N_2O)_2Cl_2$] (%): C, 38.52; H, 3.21; N, 14.98. Found: C, 38.50; H, 3.20; N, 14.96. M.P 278–280 °C; IR (KBr, cm^{-1}): 3390 [$\upsilon_{(N–H)}$], 1658 [$\upsilon_{(C=O)}$], 1542 [$\upsilon_{(C=N)\ (Py)}$].

Palladium(II) complex of 2-aminonicotinaldehyde

This complex was prepared by direct reaction between the freshly purified ligand (0.244 g, 2 mmol) and palladium(II) chloride (0.1773 g, 1 mmol) which were dissolved in 50 mL of anhydrous methanol and refluxed for 2–3 h. The color of the reaction mixture changed from pink to yellow. Yield of the complex [$Pd(C_6H_6N_2O)_2Cl_2$] 85%. Anal. Calcd. for [$Pd(C_6H_6N_2O)_2)Cl_2$] (%): C, 34.15; H, 2.84; N, 13.28. Found: C, 34.12; H, 2.80; N, 13.20. M.P 328–330 °C. IR (KBr, cm^{-1}): 3389 [$\upsilon_{(N–H)}$], 1653 [$\upsilon_{(C=O)}$], 1550 [$\upsilon_{(C=N)\ (Py)}$]. ^{1}HNMR (DMSO, ppm, 400 MHz): δ 9.85 (s, 2H, –CHO), 8.25 (d, J = 8.0, 2H), 8.01 (d, J = 8.0, 2H), 7.55 (s, 4H, –NH_2), 6.73–6.76 (m, 2H). ^{13}CNMR (DMSO, ppm, 100 MHz): δ 194.12, 158.70, 155.38, 145.04, 113.47, 112.68.

Cobalt(II) complex of 2-aminonicotinaldehyde

This complex was prepared by direct reaction between the freshly purified ligand (0.488 g, 4 mmol) and Cobalt(II) chloride hexahydrate, $CoCl_2 \cdot 6H_2O$ (0.474 g, 2 mmol) which were dissolved in 50 mL of anhydrous methanol and refluxed for 3–4 h. The color of the reaction mixture changed from pale yellow to reddish brown. At the end of the reaction, a brown solid was formed which was recrystallized from methanol, to obtain 75% yield. Anal. Calcd. For $[Co(C_6H_6N_2O)_2Cl_2]$ (%): C, 38.49; H, 3.20; N, 14.97; found: C, 38.43; H, 3.17; N, 14.92. M.P 182–185 °C. IR (KBr, cm^{-1}): 3385 [$\upsilon_{(N-H)}$], 1654 [$\upsilon_{(C=O)}$], 1512 [$\upsilon_{(C=N)\ (Py)}$].

Copper(II) complex of 2-aminonicotinaldehyde

This complex was prepared by direct reaction between the freshly purified ligand (0.488 g, 4 mmol) and copper(II) chloride, $CuCl_2$ (0.2689 g, 2 mmol) which were dissolved in 50 mL of anhydrous methanol and refluxed for 2–3 h. The color of the reaction mixture changed from pale yellow to brown. At the end of the reaction, a brownish black solid was obtained, which was recrystallized from methanol, yield 70%. Anal. Calcd. for $[Cu(C_6H_6N_2O)_2Cl_2]$ (%): C, 38.02; H, 3.16; N, 14.78; found: C, 37.99; H, 3.12; N, 14.75. M.P 218–220 °C. IR (KBr, cm^{-1}): 3391 [$\upsilon_{(N-H)}$], 1660 [$\upsilon_{(C=O)}$], 1542 [$\upsilon_{(C=N)\ (Py)}$].

Bio-assay investigations

In vitro antibacterial and antifungal activity

In vitro antibacterial and antifungal activities of the ligand and their metal complexes were tested by using the disc diffusion method. In vitro antibacterial activities have been evaluated against 2 Gram-positive bacteria (*Bacillus subtilis, Staphylococcus aureus*), 2 Gram-negative bacteria (*Klebsiella pneumoniae* and *Escherichia coli*) and two fungi strains (*Asperegillus niger*, *Pencillium notatum*). Using Whatmann No. 1 paper, 6-mm-diameter sterile antibiotic discs were placed over nutrient agar medium. By using a micropipette, 100 μg/mL of the concentrated compounds were transferred to each disc (compounds were dissolved initially in DMSO). Subsequently, the bacteria and fungi were incubated overnight at 37 and 25 °C, respectively. The zone of inhibition was determined in mm and distinguished with standard antibiotics. DMSO was used as a negative control while streptomycin 30 μg/disc (standard antibiotic) and standard antifungal drug Ketoconazole (10 μg/disc) were used as positive controls. All the tests were carried out in triplicate, and the average zones of inhibition were recorded. Minimum inhibitory concentration (MIC) values for the tested compounds as well as standards were measured in μg/mL.

In vitro DPPH free radical scavenging activity assay

The free radical scavenging activity of the synthesized ligand and its metal complexes were determined by using DPPH (1,1-diphenyl-2-picryl hydrazyl) according to the literature study [25], DPPH is a well-known radical and a scavenger for other radicals. Therefore, the DPPH radical was reduced in the presence of an anti-oxidant. In brief, 0.2 mM solution of DPPH in 100 mL methanol was prepared. Then, 3 mL of methanolic DPPH solution was added to 1 mL of ligand and its metal complexes in DMSO at different concentrations (3, 10, 30, and 100 μM). The mixture was shaken vigorously and kept in the dark at room temperature. After 30 min, the absorbance of the test compounds was measured at 517 nm using a UV–Vis spectrophotometer; methanol was used as blank. Ascorbic acid was used as standard and DPPH solution was used as control without the test compounds. The percentage of scavenging activity of DPPH free radicals was measured using the following formula.

$$\text{Scavenging activity } (\%) = \frac{A_0 - A_1}{A_0} \times 100.$$

Here A_0, is the absorbance of DPPH in the absence of an anti-oxidant and A_1, is the absorbance of DPPH in the presence of an oxidant. In addition, IC_{50} values were calculated for all compounds.

Anticancer activity

In vitro anticancer activity of the synthesized ligand and its metal complexes was evaluated against three human cancer cell lines, i.e., HeLa (human cervical carcinoma cell line), MCF-7 (human breast carcinoma cell line) and HEK293T (human embryonic kidney cell line) by using MTT colorimetric assay as per the ATCC protocol [26, 27]. *Cis*-platin was used as the standard drug. The adherent cells were trypsinized as stated by the protocol and, after centrifugation, they were resuspended in newly prepared medium. By careful pipetting, the cell suspension was mixed to obtain a homogeneous single cell suspension. Different concentrations of drug solutions were prepared in media with the final concentration of the DMSO at less than 1%. In each well of a 96-well plate, 100 μL of the cell suspension was transferred into 100 μL of 1% drug solution. This plate was incubated at 37 °C for 72 h in a CO_2 incubator. After 72 h of incubation, 20 μL of MTT was added to each well. The plate was incubated again for 2 h, then 80 μL of lyses buffer was added to each well of the plate, which was covered in aluminum foil to prevent the oxidation of the dye and placed on a shaker overnight. Absorbance was measured on an ELISA reader at 562 nm wavelength to ascertain the % inhibition of the test and also to compare with the DMSO control.

Results and discussion

The reaction leading to synthesis of ANA and its metal complexes is given in Scheme 2. The ligand ANA was prepared by the self-condensation of nicotinamide in the presence of ammonium sulfamate followed by acid-catalyzed hydrolysis. The

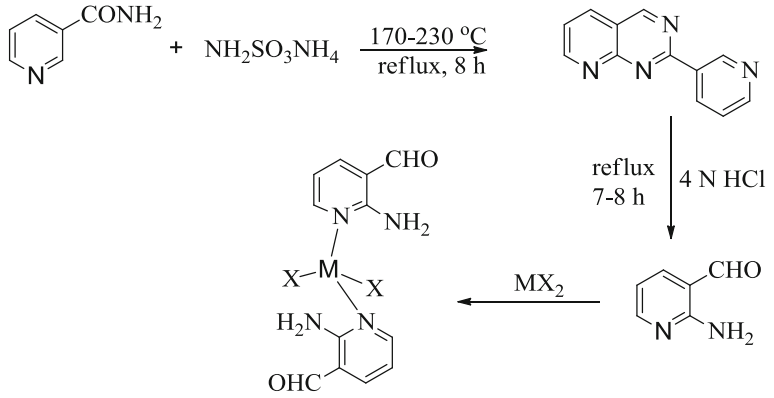

Scheme 2 The synthesis of ANA and its metal complexes M = Ni, Pd, Co and Cu, X = Cl

ligand and Pd(II) complex were also characterized by ^{1}H and ^{13}C NMR (Fig. 4a–d). Analytical data show that all the complexes have 1:2:2 (metal:ANA:chloride) stoichiometry (Table 1). The structure of the ligand was elucidated by the recrystallization of ANA in ethanol. The coordination chemistry of ANA was explored by the reaction of ANA with corresponding metal salts. Each synthetic step involved here is straightforward and provided good to moderate yield of the desired product in pure form.

IR and far-IR spectral studies

The IR spectral data of the ligand (ANA) and its metal complexes are given in Table 2. The ν_{N-H} of NH_2 of ANA occurs at 3396 cm^{-1}, the peak at 1667 cm^{-1} was assigned to $\nu_{C=O}$ of CHO group and the peak at 1575 cm^{-1} corresponds to the $\nu_{C=N}$ (py) stretching frequency of the heteroatomic ring. The IR spectra of complexes were similar to the ligand (ANA) with minor shifts in the position of the peaks. In all the spectra of the complexes, $\nu_{C=N}$ (py) peak shifted significantly to the lower wave number [28, 29], suggesting that the pyridine nitrogen of ANA is coordinated to the metal center. In the far-IR region, the new peaks at 472–421 cm^{-1} were assigned to ν_{M-N}, and at 362, 303, 296, and 290 cm^{-1} were assigned to $\nu_{M\text{-}Cl}$.

Electronic spectra

Generally, electronic absorption studies provide quick and reliable information about the geometry of metal complexes. These data can serve as an effective tool to differentiate the tetrahedral, square-planar or octahedral geometries of the transition metal complexes. The electronic spectral bands of the ligand (L) and its complexes are listed in Table 3. The UV–Vis spectrum of ANA shows two bands at 38,461 and 28,653 cm^{-1}, corresponding, respectively, to the $\pi \rightarrow \pi^*$ and $n \rightarrow \pi^*$ transitions. However, the Cu(II) complex shows a band around 24,096 cm^{-1} and a shoulder at 12,195 cm^{-1}, which may be due to $^{2}B_{1g} \rightarrow {}^{2}B_{2g}$ and $^{2}B_{1g} \rightarrow {}^{2}E_{g}$ transitions,

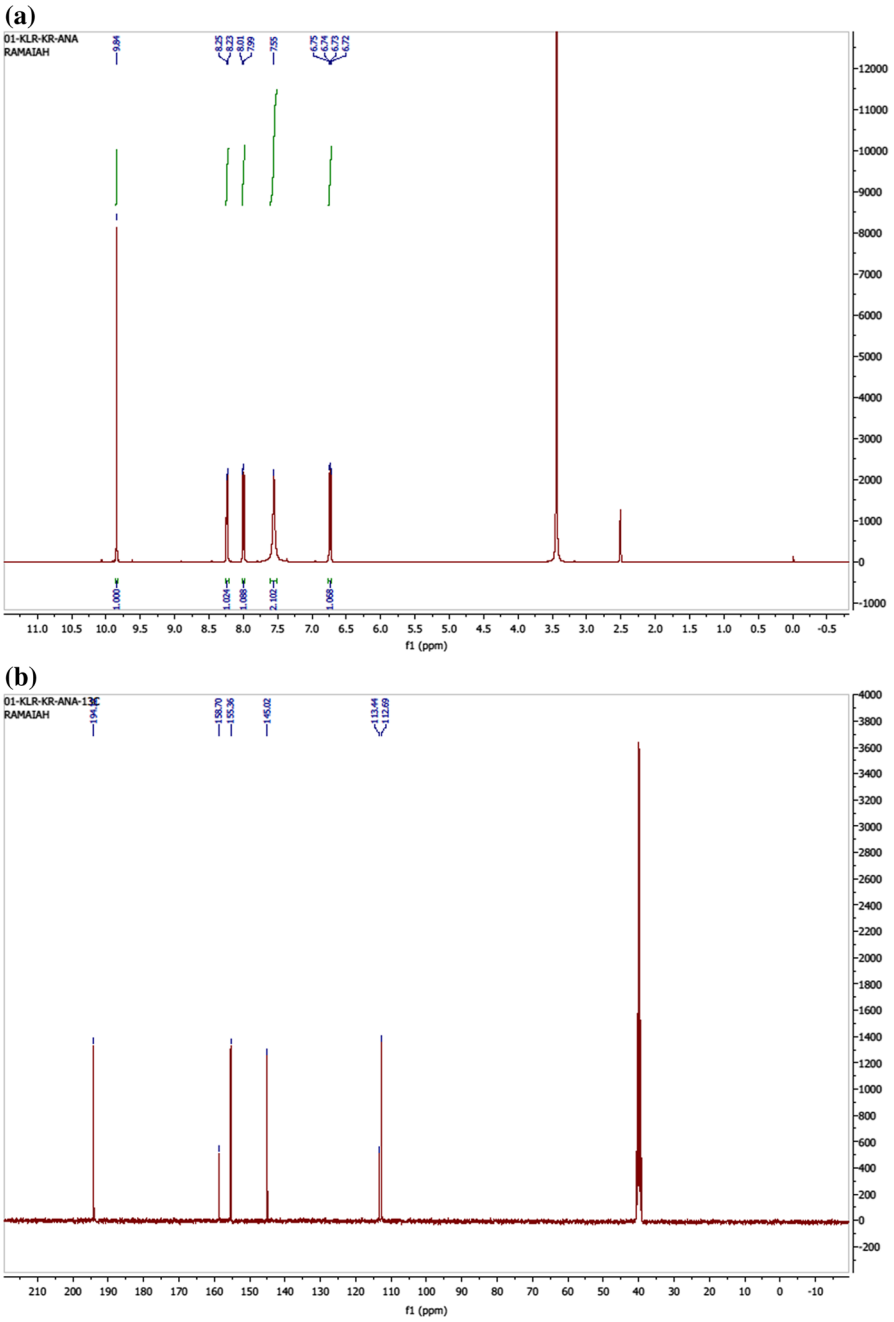

Fig. 4 **a** ^{1}H NMR and **b** ^{13}C NMR of 2-aminonicotinaldehyde (ANA), **c** ^{1}H NMR and **d** ^{13}C NMR of $[Pd(ANA)_2Cl_2]$ complex

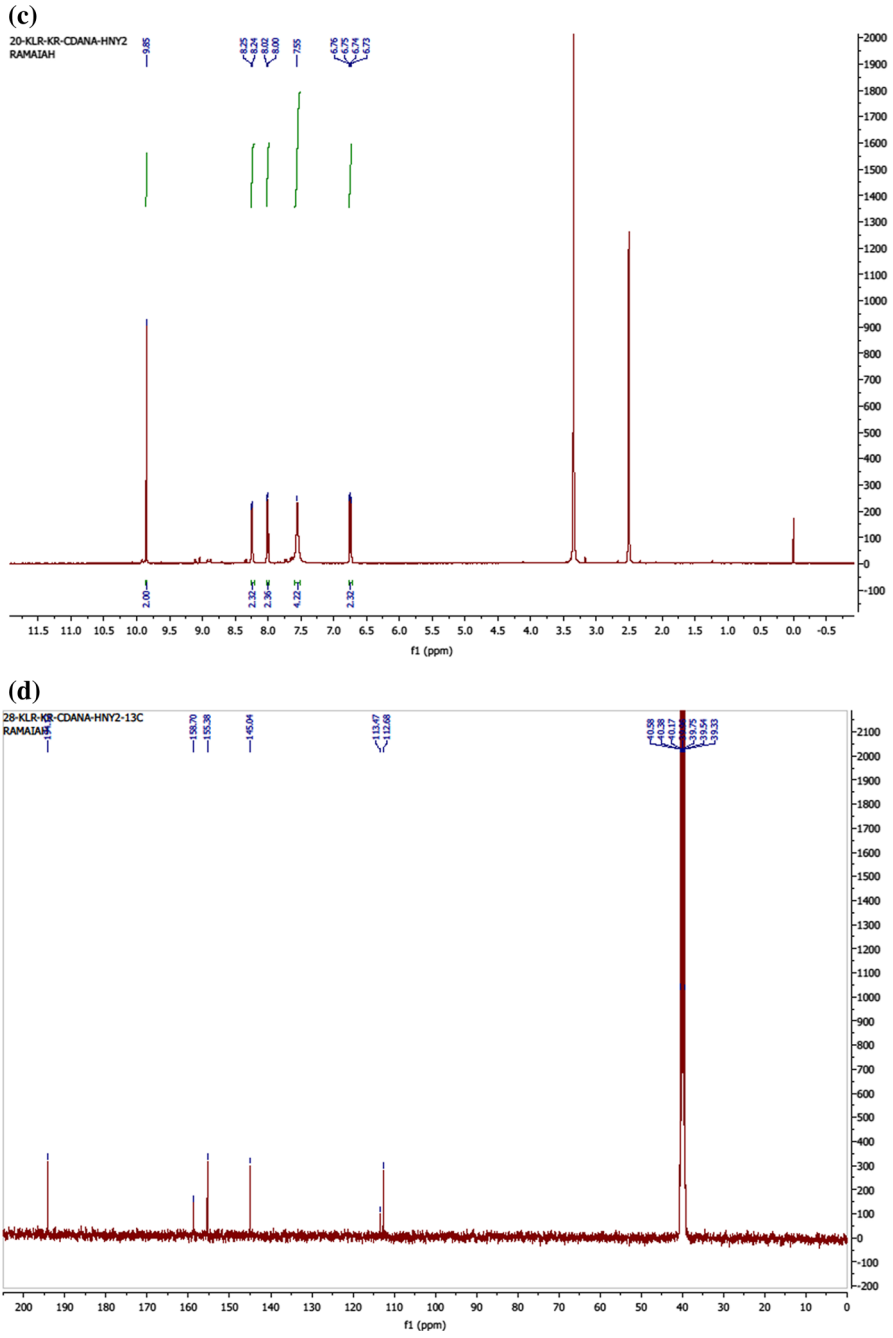

Fig. 4 continued

Table 1 Physical properties and analytical data of ligand (ANA) and its complexes

Molecular formula of ANA/complexes	Color	m.p./d.p. (°C)	Yield (%)	ESI–MS m/z (calc.)	C% found (calc.)	N% found (calc.)	H% found (calc.)	M% found (calc.)	Cl% found (calc.)
$C_6H_6N_2O$ ligand (ANA)	Yellow	99	40	122.12	58.80 (58.95)	22.87 (22.93)	4.80 (4.91)	–	–
$[Ni(C_6H_6N_2O)_2Cl_2]$	Reddish-brown	278–280	75	373.83	38.50 (38.52)	14.96 (14.98)	3.20 (3.21)	15.62 (15.69)	18.93 (18.96)
[P $[Pd(C_6H_6N_2O)_2Cl_2]$	Pale yellow	328–330	85	421.56	34.12 (34.15)	13.20 (13.28)	2.80 (2.84)	25.20 (25.24)	16.79 (16.81)
$[Co(C_6H_6N_2O)\ _2Cl_2]$	Brown	182–185	75	374.07	38.43 (38.49)	14.92 (14.97)	3.17 (3.20)	15.70 (15.75)	18.90 (18.95)
$[Cu(C_6H_6N_2O)\ _2Cl_2]$	Brownish-black	218–220	70	378.68	37.99 (38.02)	14.75 (14.78)	3.12 (3.16)	16.75 (16.77)	18.70 (18.72)

Table 2 IR and far-IR spectral data (cm^{-1})

Compound	ν_{N-H}	$\nu_{C=O}$	$\nu_{C=N(py)}$	ν_{M-N}	ν_{M-Cl}
Ligand (ANA)	3396	1667	1575	–	–
$[Ni(ANA)_2Cl_2]$	3390	1658	1542	472	362
$[Pd(ANA)_2Cl_2]$	3389	1653	1550	446	303
$[Co(ANA)_2Cl_2]$	3385	1654	1512	451	296
$[Cu(ANA)_2Cl_2]$	3391	1660	1542	421	290

Table 3 Electronic spectral data of the ligand and its metal complexes

Compound	Band position (cm^{-1})	Transition	Geometry
ANA	28,653	n → π*	
	38,461	π → π*	
$[Ni(ANA)_2Cl_2]$	9500	^{3}T1(F) → 3A2(F)	Tetrahedral
	19,157	3T1(F) → 3T1(P)	
$[Pd(ANA)_2Cl_2]$	22,540	^{1}A1g → 1Eg	Square planar
	31,750	Charge transfer	
$[Co(ANA)_2Cl_2]$	9000	4A2(F) → 4T1(F)	Tetrahedral
	20,400	4A2(F) → 4T1(P)	
$[Cu(ANA)_2Cl_2]$	12,195	2B1g → 2Eg	Square planar
	24,096	2B1g → 2B2g	

respectively, characteristic of square-planar geometry [30]. The UV–Vis spectrum of the Co(II) complex usually shows three bands in the regions 3000–5000, 6000–10,000 and 15,000–21,000 cm^{-1}, which may be assigned to $^4A_2(F) \rightarrow {}^4T_2(F)$, $^4A_2(F) \rightarrow {}^4T_1(F)$ and $^4A_2(F) \rightarrow {}^4T_1(P)$ transitions, respectively. However, in the present Co(II) complex, the latter two bands, observed at around 9000 and 20,400 cm^{-1}, are characteristic of tetrahedral geometry [31]. The Pd(II) complex exhibits two bands around 22,540 and 31,750 cm^{-1}, which may be assigned to $^1A_{1g} \rightarrow {}^1E_g$ and charge transfer transitions, respectively, characteristic of square-planar geometry [32]. The Ni(II) complex is found to be paramagnetic and its absorption spectrum showed two bands around 9500 and 19,157 cm^{-1}, which could be assigned to $^3T_1(F) \rightarrow 3A_2(F)$ and $^3T_1(F) \rightarrow 3T_1(P)$ transitions, respectively, which were orderly with reported tetrahedral geometry [33].

Square-planar Cu(II) complexes show magnetic moment values in the range of 1.8–2.1 BM. These values are somewhat greater than the spin-only value of 1.73 BM and this is due to the spin–orbit coupling followed by lowering of symmetry [34]. The magnetic moment of the Cu(II) complex is observed as 2.01 BM which also supports square-planar geometry around the metal ion [35]. The magnetic moment of the Co(II) complex is 3.87 BM which suggests the paramagnetic tetrahedral geometry of the complex molecule, while the Ni(II) complex is also paramagnetic and the magnetic moment at room temperature is found to be 2.91 BM, well in agreement with tetrahedral geometry [36]. The Pd(II) complex is

diamagnetic in nature, and, based on this, square-planar geometry has been proposed [37].

To study the thermodynamic stability of the complexes in aqueous medium, a series of parts were prepared with suspensions of 10 mg of the complexes in 20 mL of water in each part. In UV–Vis spectra of the filtrate of each part at various time intervals (60 s, 1 h, 5 h, 10 h and 12 h), the spectral patterns were found to be invariant with the time of suspension, which indicates that the complexes were thermodynamically stable in aqueous medium. The same trend was observed in the buffer medium in which biological studies were made.

Cyclic and differential pulse voltammograms

The cyclic (CV) and differential pulse (DPV) voltammograms of all the metal complexes were recorded in CH_3CN (containing 0.1 M TBAP) (Fig. 5). The values obtained were calibrated with respect to the Fc^+/Fc couple. $[Cu(ANA)_2Cl_2]$ showed a reversible ($ip_c/ip_a = 0.9–1.0$) and diffusion-controlled [$ip_c/v^{1/2}$ = constant in the scan rate (v) range 50–500 mV/s] one-electron transfer ($\Delta Ep = 60–70$ mV; $\Delta Ep = 65 \pm 3$ mV for Fc^+/Fc couple) couple at -181 mV. On the other hand, $[Co(ANA)_2Cl_2]$ showed an irreversible peak at 967 mV, whereas the Ni(II) complex of ANA was observed to be electrochemically silent, as expected. The irreversible oxidative peak observed at this potential cannot be attributed to the oxidation to Co(II) to Co(III) because the standard reduction potential of Co(III)/Co(II) is +1.81. Hence, this voltammetric irreversible oxidative peak is assigned to the removal of an electron from the lone pair of electrons available on one of the two NH_2 groups of the otherwise chemically equivalent ligand molecules.

NMR spectral studies

^{1}H NMR spectra of ANA were recorded in DMSO-d_6, with signals at δ 9.84 ppm (s, 1H), 8.24 ppm (d, $J = 8.0$ Hz, 1H), 8.00 ppm (d, $J = 8.0$ Hz, 1H), 7.55 ppm (s, 2H, $–NH_2$), 6.72–6.75 ppm (m, 1H). The ^{13}C NMR spectrum of ANA exhibits

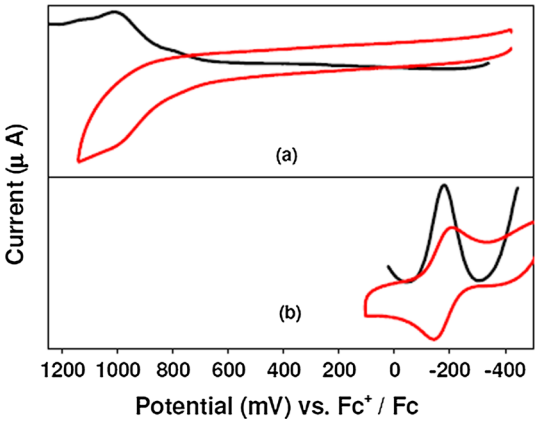

Fig. 5 Cyclic and differential pulse voltamograms of **a** $[Co(ANA)_2Cl_2]$ and **b** $[Cu(ANA)_2Cl_2]$ in CH_3CN

signals from 112.69 to 194.12 ppm. The signal at 194.12 ppm is assigned to aldehyde carbon, the peaks at 155.36 ppm and 112.69 ppm are due to quaternary carbons and the peaks at 113.44, 145.02 and 158.70 ppm are for the remaining carbons. These peaks in the spectra of the complex appeared with positive coordination-induced shifts, indicating that the pyridine N of ANA is involved in bonding with the metal ion.

Crystal structure of ANA

The single-crystal data of ANA are listed in Table 4. The crystallized in the monoclinic system, with space group $P2_1/c$ with Z = 8. In the crystal structure, an asymmetric unit consists of two molecules of ANA, labeled separately as A and B with the atom-numbering shown in Fig. 6. The classical intramolecular hydrogen bonding of N–H···O (N_2–H_2a···O1 and N_4–H_2a···O2) and intermolecular hydrogen bonding of N–H···N (N_2–H_2b…..N_1 and N_4–H_4b···N3) leads to the formation of dimeric units of molecules of B and herring bone stacking of molecules of A along the *b*-axis (Fig. 7a, b). Furthermore, the non-classical inter-molecular hydrogen bonding of C–H…..N/O between dimeric units of molecules (C_3–H_3···O_2 and C_{10}–H_{10}···N_3) as a result of glide plane gives rise to a different type of herring bone stacking pattern of molecules expanded on two dimensions (Fig. 7c). In addition to this hydrogen bonding, the aldehyde hydrogen H_{12}, aromatic ring carbon hydrogens H_4 and H_9 are also involved in trifurcated hydrogen bonding with O_1, which connects the molecules together in the crystal structure Fig. 8. The aromatic rings are further stabilized by weak displaced π–π interaction (3.955Å). The overall intermolecular non-covalent interactions and packing diagram of the molecules extended in two dimensions are shown in Fig. 9. In a nutshell, the three-dimensional network of ANA consists of classical and non-classical hydrogen bonding networks for its 3D architecture (Fig. 10). The H-binding data of ANA are listed in Table 5.

Electron spin resonance

The electron spin resonance spectrum of the Cu(II) complex was recorded in benzene solution at room temperature in the solid state (Fig. 11). It shows a broad band centered at $g = 2.21$, without a resolved hyperfine structure with the values $g_{\|} = 2.144$ and $g_{\perp} = 2.087$. The $g_{\|} > g_{\perp} > 2.0023$, showing that the unpaired electron in the ground state of Cu(II) predominantly lies in the $d^2_X - {}^2_Y$ orbital and also refere to a square-planer geometry around the Cu(II) ions [38]. The observed $g_{\|}$ value of the metal complex is less than 2.3, which is in agreement with the covalent character of the metal ligand bond [39]. The geometric parameter *G* is calculated using the equation:

$$G = \frac{g_{\|} - 2.0023}{g_{\perp} - 2.0023}.$$

According to Hathaway and Billing [40, 41], if the value of *G* is greater than 4, this indicates that the exchange interaction between the Cu(II) centers in the solid state

Table 4 Crystallographic data of ANA

Compound	Ligand (ANA)
Empirical formula	$C_6H_6N_2O$
Formula weight	122.13
Wavelength (Å)	0.71073
Crystal system	Monoclinic
Space group	$P2_1/c$
a (Å)	22.8474 (14)
b (Å)	3.9552 (2)
c (Å)	13.1652 (8)
α (°)	90
β (°)	94.465 (4)
γ (°)	90
Volume ($\mathring{A}^3$)	1186.1 (1)
Z	8
$D_{calc.}$ ($M_g^{-3}{}_m$)	1.368
Temperature (K)	296
Absorption coefficient (mm^{-1})	0.097
F (000)	512
Crystal size (mm^3)	0.23 × 0.20 × 0.18
θ range for data collection (°)	0.89–25.99
Reflections collected/unique	12,978/2321
Completeness to θ	25.99, 100%
Independent reflections (R_{int})	0.1902
Max./min. transmission	0.9827/0.9779
Data/parameters	2321/212
Goodness-of-fit on F^2	0.881
Final *R* indices[I > 2σ(I)]	$R_1 = 0.0497$[a]
	$wR_2 = 0.1071$[b,c]
R indices(all data)	$R_1 = 0.0733$[a]
	$wR_2 = 0.1152$[b,c]
Extinction coefficient	0.044 (4)
Largest diff. peak and hole ($e\bar{\mathring{A}}^3$)	0.235 and −0.235

[a] $R_1 = \sum(|F_O| - |F_C|)/\sum|F_O|$

[b] $wR_2 = \{\sum [w\,(F_O^2 - F_C^2)^2]/\sum [w(F_O^2)^2]\}^{1/2}$

[c] $w = 1/[\sigma^2(F_O^2) + (aP)^2 + bP]$ with $P = [F_o^2 + 2F_c^2]/3$

$a = 0.0333$ and $b = 0.000$ for ANA

is negligible, whereas when its value is less than 4, considerable exchange interactions exist in the solid complex. The value $G = 1.672$ for the exchange interaction parameter for the Cu(II) complex is less than 4, indicating that there is a spin exchange interaction between Cu(II) ions in the solid state.

Antibacterial activity

The in vitro antibacterial evaluation results reveal that the ligand ANA does not show any activity against the strains, the complexes $[Cu(ANA)_2Cl_2]$ and $[Co(ANA)_2Cl_2]$ exhibited good activity against *S. aureus* (12.5 μg/mL) and

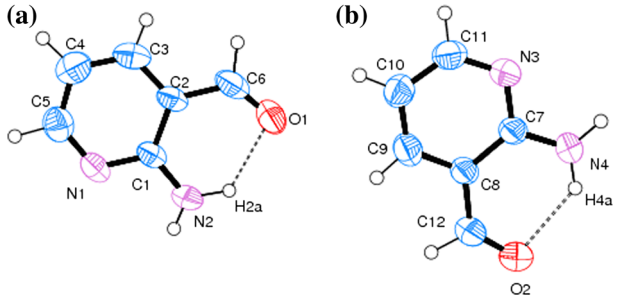

Fig. 6 ORTEP diagram of ligand up to 50% probability showing intramolecular N–H···O hydrogen bonds (with atom numbering)

moderate activity against three strains, *B. subtilis* (25 μg/mL), *E. coli* (25 μg/mL) and *K. pneumoniae* (25 μgmL). The complexes $[Ni(ANA)_2Cl_2]$ and $[Pd(ANA)_2Cl_2]$ exhibited poor activity against *S. aureus*, *B. subtilis*, *E. coli* and *K. pneumoniae* compared to the standard drug streptomycin. ANA does not show any activity, whereas the activity of the $[Cu(ANA)_2Cl_2]$ and $[Co(ANA)_2Cl_2]$ complexes against four strains may be attributed to the coordination of ANA with metals. The MIC of the complexes are presented in Table 6. In conclusion, $[Co(ANA)_2Cl_2]$ and $[Cu(ANA)_2Cl_2]$ complexes showed good activity against *S. aureus* and moderate activity against *B. subtilis*, *E. coli* and *K. pneumoniae* in comparision with the $[Ni(ANA)_2Cl_2]$ and $[Pd(ANA)_2Cl_2]$ complexes.

Antifungal activity

ANA and its metal complexes were investigated for in vitro antifungal activity against the fungal strains *Aspergillus niger* and *Pencillium notatum*, and compared with the standard drug Ketoconazole with MIC values. The results of the in vitro antifungal activity in MIC of the tested compounds are presented in Table 7 in which it can be seen that the complexes $[Cu(ANA)_2Cl_2]$ and $[Co(ANA)_2Cl_2]$ exhibited very good activity against *Aspergillus niger* and *Pencillium notatum*, with IC_{50} values (6.25 and 6.25 μg/mL) and (6.25 and 12.5 μg/mL), respectively. The complexes $[Ni(ANA)_2Cl_2]$ and $[Pd(ANA)_2Cl_2]$ exhibited moderate to poor activity against the strains, with IC_{50} values (50 and 50 μg/mL) and (50 μg/mL). The ligand ANA had no activity, but its complexes $[Cu(ANA)_2Cl_2]$ and $[Co(ANA)_2Cl_2]$ showed good activity.

The metal ion and ligand association exerts a synergistic effect on the activity of the free ligand [42, 43]. The metal ion–ligand interaction in the complexes leads to the activity of changing the electron distribution in the ligand. In conclusion, $[Co(ANA)_2Cl_2]$ and $[Cu(ANA)_2Cl_2]$ complexes showed potent activity against *Aspergillus niger* and *Pencillium notatum*, in comparison with the $[Ni(ANA)_2Cl_2]$ and $[Pd(ANA)_2Cl_2]$ complexes.

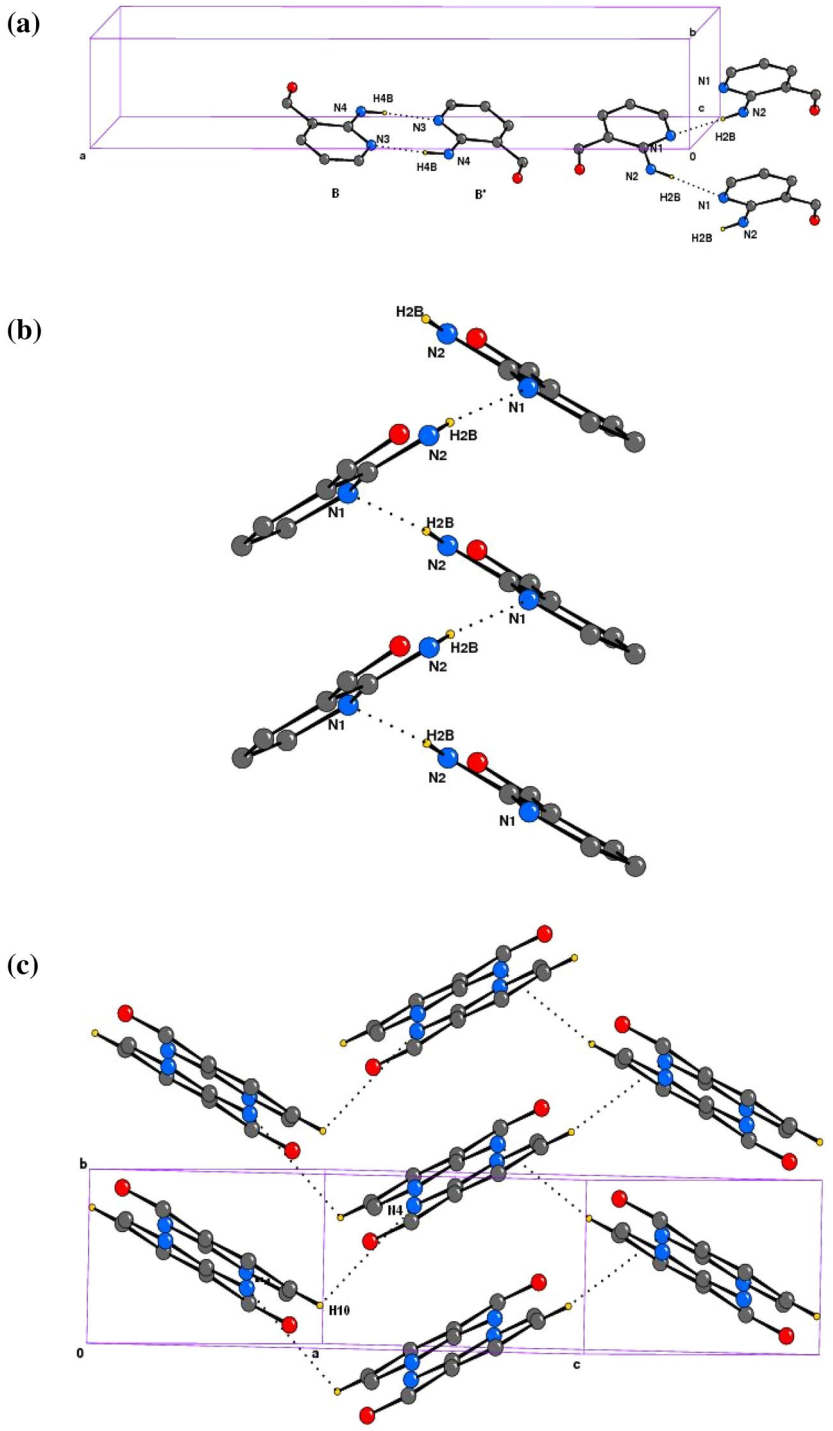
(a)
b
a
c
0
N4
H4B
N3
N3
H4B
N4
B
B'
N1
N2
H2B
N1
N2
H2B
N2
H2B
N1
(b)
H2B
N2
N1
H2B
N2
N1
H2B
N2
N1
H2B
N2
N1
(c)
b
0
a
c
H4
H10

◀**Fig. 7** **a** Intermolecular interactions of the ligand ANA, intermolecular hydrogen bonding depicting dimer formation of B and herring bone pattern formation A. **b** Herring bone stacking pattern of molecule A along *b* axis. **c** Herring bone pattern of dimeric units of molecules B

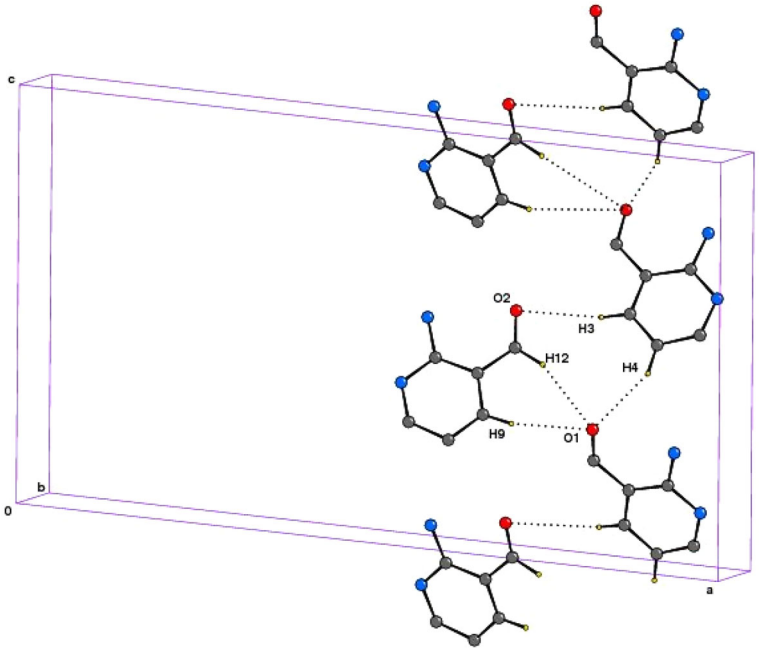

Fig. 8 Intermolecular non-classical hydrogen bonding between molecules A and B

Antioxidant activity

The IC_{50} values of the ligand and its metal complexes are given in Table 8. It can be seen that, by increasing the concentration of the compounds, the scavenging activity also increases. The DPPH assay of the metal complexes (1–4) was calculated as percentage inhibition (Fig. 12). From the results, it is shown that the scavenging effect of the free ligand is significantly less compared to the metal complexes [25]. The antioxidant activity of the complexes $[Ni(ANA)_2Cl_2]$ and $[Cu(ANA)_2Cl_2]$ show better activity with IC_{50} values at 12.39 ± 1.26 and 14.82 ± 1.27 μM, respectively. Analogues $[Pd(ANA)_2Cl_2]$ and $[Co(ANA)_2Cl_2]$ complexes showed moderate activity with IC_{50} values, 16.27 ± 1.19 and 19.49 ± 1.30 μM, respectively. According to IC_{50} values, the scavenging activity order of the compounds follows:

$$[Ni(ANA)_2Cl_2] > [Cu(ANA)_2Cl_2] > [Pd(ANA)_2Cl_2] > [Co(ANA)_2Cl_2] > ANA.$$

In conclusion, the complexes $[Ni(ANA)_2Cl_2]$ and $[Cu(ANA)_2Cl_2]$ complexes have shown good anti-oxidant activity compared to the $[Pd(ANA)_2Cl_2]$ and $[Co(ANA)_2Cl_2]$ complexes.

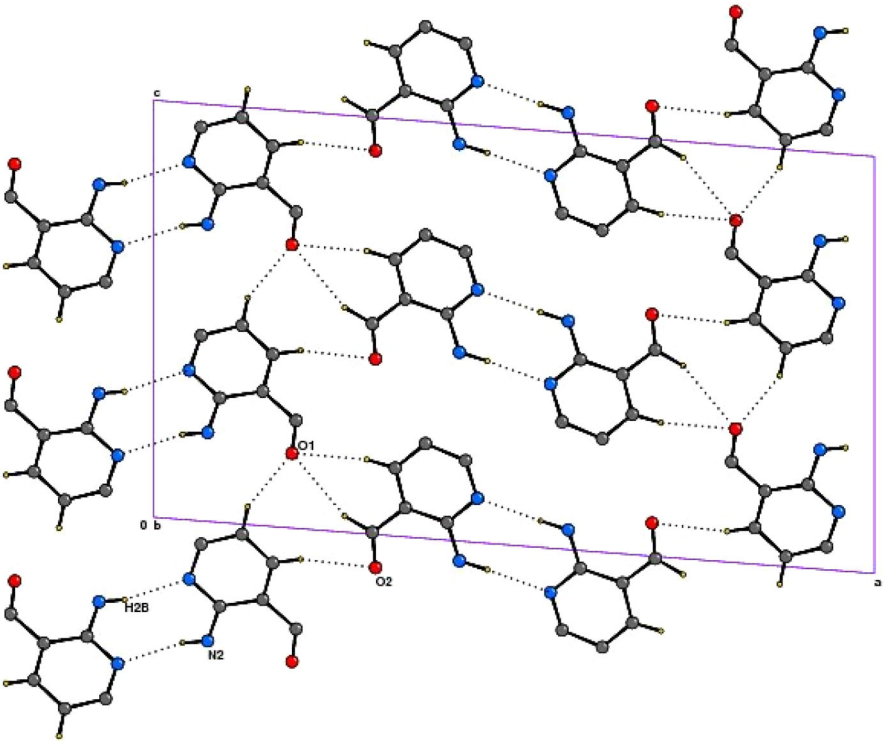

Fig. 9 Two-dimensional stacking diagram depicting the intermolecular H-bonding

Anticancer activity

The ligand and its metal complexes were evaluated against HeLa, MCF-7 and HEK-293T using MTT assay, with *cis*-platin is used as standard drug. The relationship between the surviving fraction and drug concentration was plotted to obtain the survival curves of HeLa, MCF-7 and HEK 293T (Fig. 13a–c). The IC_{50} values calculated for the synthesized compounds against the tested cell lines are listed in Table 9. The results show that the $[Ni(ANA)_2Cl_2]$ complex exhibited good activity against the three cancer cell lines, with IC_{50} values 26.40 ± 0.29, 22.86 ± 0.29 and 34.23 ± 0.27 μM, respectively, compared with the standard drug *cis*-platin. The $[Pd(ANA)_2Cl_2]$ complex showed good activity against the HeLa cell line with IC_{50} values 27.48 ± 0.20 μM, the $[Co(ANA)_2Cl_2]$ complex showed good activity against the MCF-7 cell line with IC_{50} values 27.48 ± 0.12 μM and $[Cu(ANA)_2Cl_2]$ complex showed significant activity against the two cell lines, HeLa and MCF-7, with IC_{50} values 29.04 ± 0.37 and 31.26 ± 0.18 μM, respectively. The metal complexes were also screened for cytotoxic activity against HEK-293. IC_{50} values of the $[Pd(ANA)_2Cl_2]$, $[Co(ANA)_2Cl_2]$ and $[Cu(ANA)_2Cl_2]$ complexes were

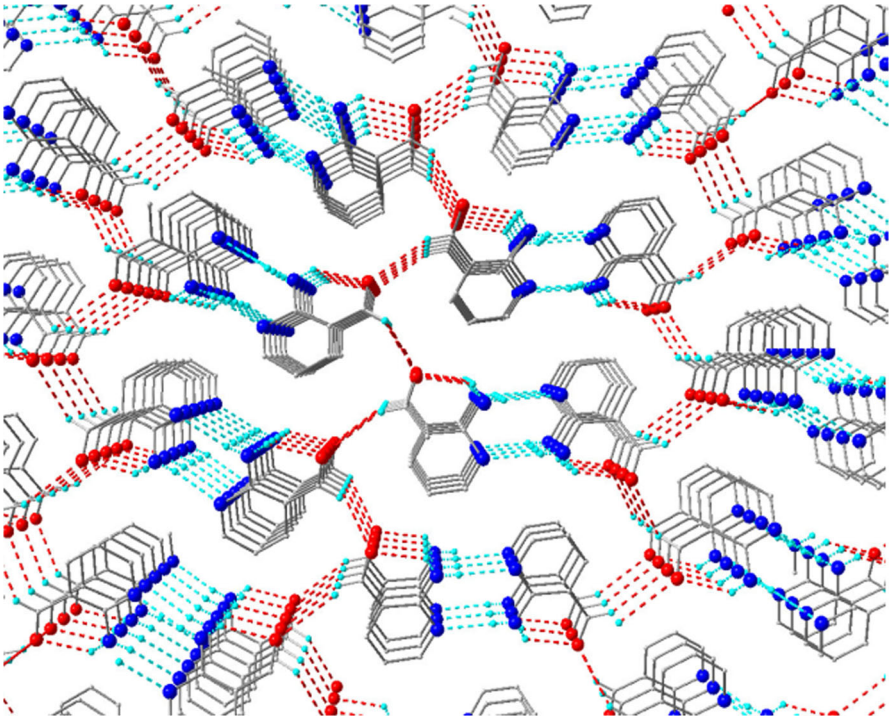

Fig. 10 3D-crystal structure of ANA

Table 5 Hydrogen-bond parameters of ANA

Compound	D–H…A	D–H	D···A	H····A	<D–H····A	Symmetry code
ANA	N_2–H_2a···O_1	1.00 (2)	2.745 (2)	2.02 (2)	127 (2)	*x, y, z*
	N_4–H_4a···O_2	0.97 (2)	2.781 (2)	2.06 (3)	130 (2)	*x, y, z*
	C_3–H_3···O_2	0.91 (2)	3.662 (2)	2.79 (2)	158 (2)	$x, y - 1, z + 1$
	C_4–H_4···O_1	0.98 (2)	3.538 (3)	2.61 (2)	154 (2)	$x, -y + 1/2, z + 1/2$
	C_{10}–H_{10}···N_4	0.96 (2)	3.666 (2)	2.88 (2)	138 (1)	$x, -y + 1/2, z + 1/2$
	C_9–H_9···O_1	0.94 (2)	3.472 (2)	2.57 (2)	159 (2)	$x, -y + 1/2 + 1, z - 1/2$
	C_{12}–H_{12}···O_1	1.01 (2)	3.558 (3)	2.59 (2)	159 (2)	$-x, -y + 1/2 + 1, z - 1/2$
	N_4H_4b···N_3	0.92 (2)	3.073 (2)	2.14 (2)	176 (2)	$-x + 1, -y + 1, -z$
	N_2–H_2b···N1	0.84 (2)	3.082 (2)	2.25 (2)	167 (2)	$-x, y + 1/2, -z = 1/2 + 1$

72.32 ± 0.21, 40.58 ± 0.20 and 44.74 ± 0.35 μM, respectively. The results are presented in Table 9. In conclusion, the $[Ni(ANA)_2Cl_2]$ complex showed good activity against HeLa, the MCF-7. $[Pd(ANA)_2Cl_2]$ complex against HeLa and the $[Co(ANA)_2Cl_2]$ complex against MCF-7.

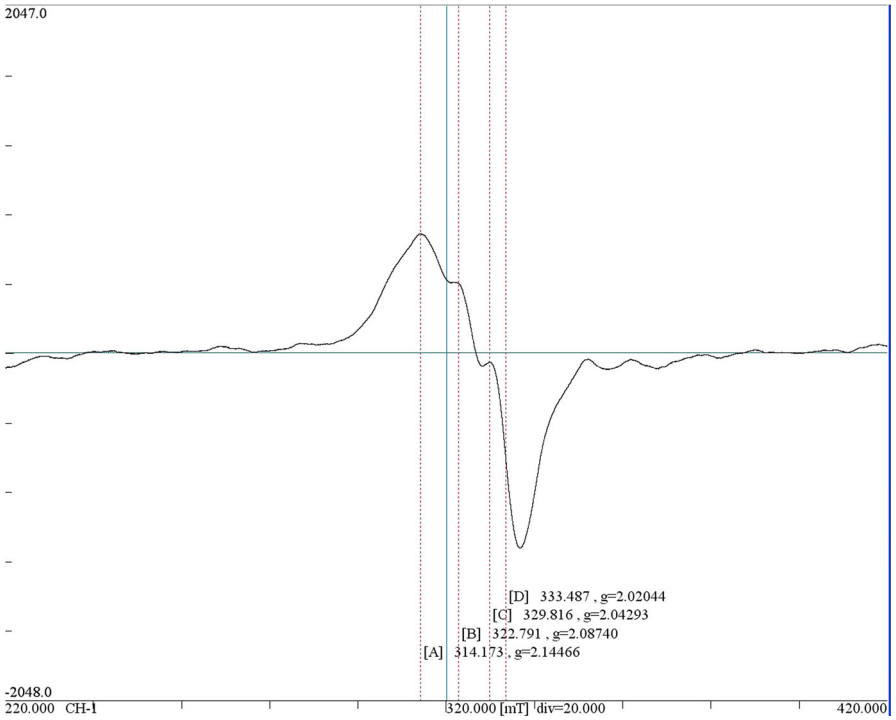

Fig. 11 ESR spectrum of the Cu(II) complex

Table 6 Antibacterial activity of the compounds MIC (μg/mL)

MIC (μg/mL)				
Compound	*S. aureus*	*B. subtilis*	*K. pneumoniae*	*E. coli*
ANA	>100	>100	>100	>100
$[Ni(ANA)_2Cl_2]$	50	100	>100	50
$[Pd(ANA)_2Cl_2]$	100	50	>100	50
$[Co(ANA)_2Cl_2]$	12.5	25	25	50
$[Cu(ANA)_2Cl_2]$	12.5	25	25	25
Streptomycin	6.25	12.5	12.5	6.25

Molecular docking studies

Our aim was to explain the interactions of metal complexes with protein receptors, and we have chosen a computer-aided experimental method, molecular docking. Chem Draw Ultra 12.0 has been used to draw the 2D structures of the metal complexes and the structures have been fully optimized with the small hf/3–21 g* [44], basic set by using Guassian 09 [45]. The crystallographic 3D structure of the EGFR protein receptor was retrieved from RSC PDB (an information portal for

Table 7 Antifungal activity of the compounds (MIC (μg/mL)

MIC (μg/mL)		
Compound	*Asperegillus niger*	*Pencillium notatum*
ANA	>100	>100
$[Ni(ANA)_2Cl_2]$	50	50
$[Pd(ANA)_2Cl_2]$	50	>100
$[Co(ANA)_2Cl_2]$	6.25	12.5
$[Cu(ANA)_2Cl_2]$	6.25	6.25
Standard(Ketoconazole)	3.125	3.125

Table 8 IC_{50} (μM) values of DPPH scavenging activity of ligand and its metal complexes

Sample no.	Compound codes	IC_{50} (μM)
1	$[Ni(ANA)_2Cl_2]$	12.39 ± 1.26
2	$[Pd(ANA)_2Cl_2]$	16.27 ± 1.19
3	$[Co(ANA)_2Cl_2]$	19.49 ± 1.30
4	$[Cu(ANA)_2Cl_2]$	14.82 ± 1.27
5	ANA	20.60 ± 1.38
6	(Standard) Ascorbic Acid	6.53 ± 1.19

Order of reactivity: 1 > 4 > 2 > 3 > 5

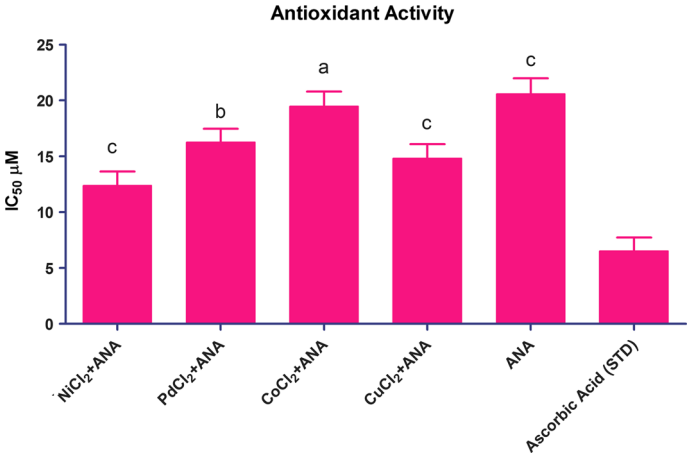

Fig. 12 Radical scavenging activity of ligand and metal complexes in terms of IC_{50} value (50% inhibition): *Letters over columns*:[a] $p < 0.05$, [b] $p < 0.01$, [c] $p < 0.001$ and $p > 0.05$ as non-significant. It was determined by unifactorial analysis of variance (ANOVA) followed by Dunnett's multiple comparison test using Graphpad Prism Software v.5.3

biological macromolecular structures), PDB ID: 4HJO. It is an attractive target in cancer disease. EGFR plays a major role in the causing of cancer including squamous-cell carcinoma of the lung, anal cancers, and epithelia tumors of the head and neck [46] in the human body. Mutations involving EGFR lead to its constant

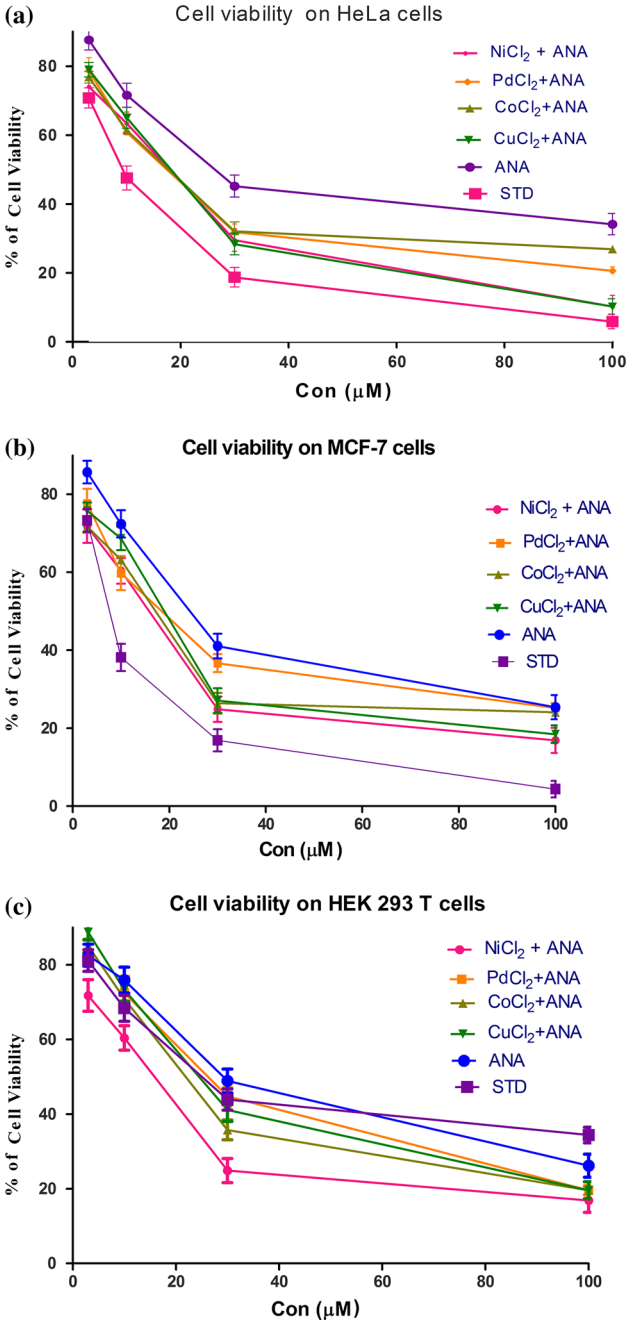

Fig. 13 Survival curves of HeLa, MCF-7 and HEK293 T cell lines. **a** Anticancer activity (HeLa), **b** anticancer activity (MCF-7), **c** anticancer activity (HEK293)

Table 9 IC_{50} values of anticancer activity of compounds (μM)

Sample no.	Compound codes	IC_{50} values (μM)		
		HeLa	MCF-7	HEK 293T
1	$[Ni(ANA)_2Cl_2]$	26.40 ± 0.29	22.86 ± 0.29	34.23 ± 0.27
2	$[Pd(ANA)_2Cl_2]$	27.48 ± 0.20	40.580 ± 0.30	72.32 ± 0.21
3	$[Co(ANA)_2Cl_2]$	34.23 ± 0.31	27.48 ± 0.12	40.58 ± 0.20
4	$[Cu(ANA)_2Cl_2]$	29.04 ± 0.37	31.26 ± 0.18	44.74 ± 0.35
5	ANA	56.26 ± 0.49	46.86 ± 0.28	51.03 ± 0.41
6	Standard (*Cis*-platin)	10.14 ± 0.17	4.77 ± 0.16	52.56 ± 0.39

Table 10 Binding energies of metal complexes with EGFR protein receptor (4HJO)

Sample no.	Compound	Binding energy (K cal/mol)
1	$[Co(ANA)_2Cl_2]$	−4.16
2	$[Ni(ANA)_2Cl_2]$	−4.64
3	$[Cu(ANA)_2Cl_2]$	−4.88
4	$[Pd(ANA)_2Cl_2]$	−5.46

activation, and it develops uncontrolled cell division [47]. The extracted protein structures were prepared by removing water molecules and minimizing the energy of the protein receptor with UCSF chimera 1.10.1 software used for docking. The metal complexes $[Co(ANA)_2Cl_2]$, $[Ni(ANA)_2Cl_2]$, $[Cu(ANA)_2Cl_2]$ and $[Pd(ANA)_2Cl_2]$ were bound to the receptor with minimum binding energies −4.16, −4.64, −4.88 and −5.46 K cal/mol, respectively. The docking results were compared with the experimental IC_{50} values in Table 10. The best conformations of ligands forming a cluster into the binding pocket of the receptor are shown in Fig. 14a–d. From these results, we can conclude that, in the protein EGFR complex, all the interactions of the $[Co(ANA)_2Cl_2]$ complex are hydrophobic interactions with amino acids, Ser167, Tyr126, Ser267, Glu171, His346, Phe214, Phe270, Phe163, Val170, and Ala264. In the $[Ni(ANA)_2Cl_2]$-protein receptor complex, all the similar interactions were found with the amino acids, Phe699, Asp813, Ala698, Phe699, Lys721, Asp813, Asn818, Lys851, Pro853, and Arg817. In the $[Cu(ANA)_2Cl_2]$ protein receptor complex, the same kind of interactions were found with amino acids, Arg817, Asn818, Asp813, Asp831, Ala698, and Pro853. In addition to these interactions, π–π stacking interactions were observed.

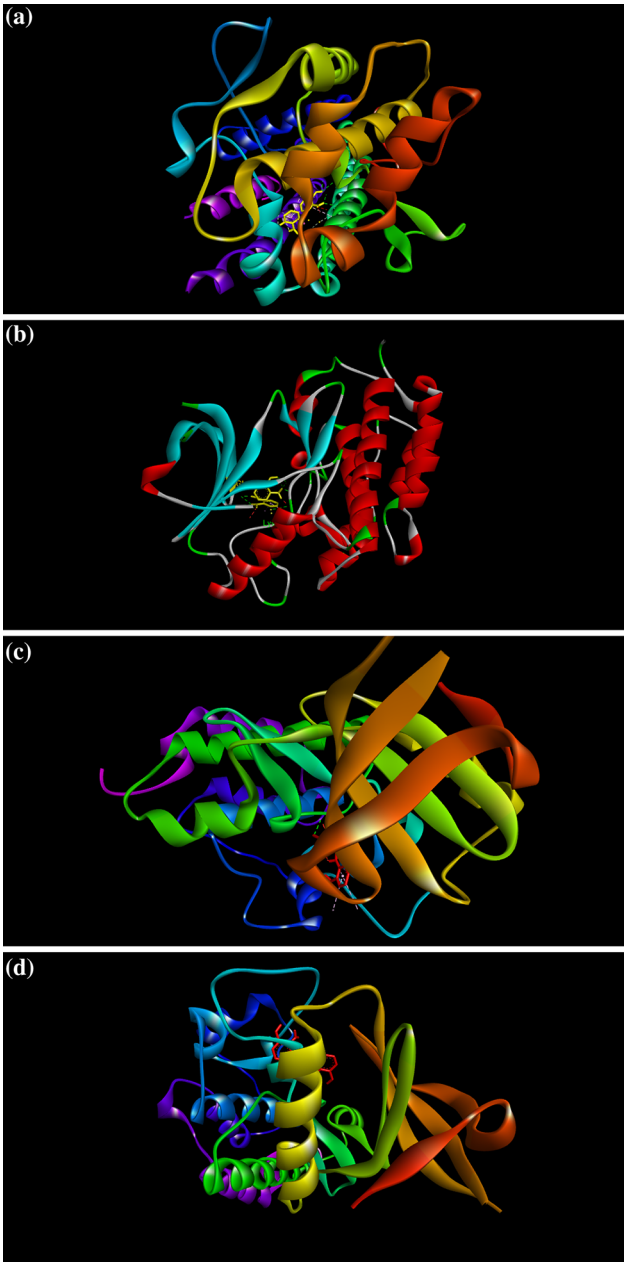

Fig. 14 a–d Shows the binding process and interactions of metal complexes of $[Co(ANA)_2Cl_2]$, $[Ni(ANA)_2Cl_2]$, $[Cu(ANA)_2Cl_2]$ and $[Pd(ANA)_2Cl_2]$ to the binding sites of the EGFR protein receptor

Conclusions

We have, for the first time, demonstrated the coordination behavior of 2-aminonicotinaldehyde with transition metals Ni(II), Pd(II), Co(II) and Cu(II). The ligand ANA and its metal complexes have been synthesized and characterized by using various spectroscopic techniques. ANA acts as a mono-dentate ligand towards the metal ions through the N atom of the pyridine ring, orienting the aldehyde and amine potential functional groups of the ligand in the metal complexes. Based on these studies, the structures of the Pd(II) and Cu(II) complexes may be tentatively proposed as having square-planar geometry, whereas the Ni(II) and Co(II) complexes show tetrahedral geometry with the $[M(N)_2(Cl)_2]$ coordination sphere. The biological activity may be specific due to metal–ligand orientations facilitating hydrophobic interactions and π–π stacking in the protein receptor complex. The metal complexes Co(II) and Cu(II) were potent antibacterial and antifungal agents. The Ni(II) complex showed the highest scavenging activity and displayed good anticancer activity against the HeLa, MCF-7 and HEK 293 human cancer cell lines, compared with other metal complexes.

Supplementary material

CCDC 801685 contains the supplementary crystallographic data of ligand ANA. The data can be obtained free of charge via http://www.ccdc.cam.ac.uk/conts/retrieving.html, or from the Cambridge Crystallographic Data Centre, 12 Union Road, Cambridge, CB2 1EZ, UK; fax: (+44) 1223-336-033; or e-mail: deposit@ccdc.cam.ac.uk.

Acknowledgements I am very grateful to Dr. Munirathinam, IISC Bangalore, for providing the single-crystal XRD facility. I am grateful to the Ministry of Human Resource Development (MHRD), India for awarding a research fellowship to me.

References

1. X. Lin, J.H. Jia, X.B. Zhao et al., Angew. Chem. Int. Ed. **45**, 7358 (2006)
2. B. Moulton, M.J. Zaworotko, Chem. Rev. **101**, 1629 (2001)
3. H. Furukawa, M.A. Miller, O.M. Yaghi, J. Mater. Chem. **17**, 3197 (2007)
4. H. Li, M. Eddaoudi, M.O. Keeffe, O.M. Yaghi, Nature **402**, 276 (1999)
5. D. Braga, L. Brammer, N.R. Champneess, Cryst. Eng. Comm. **7**, 57 (2005)
6. P. Metranglo, F. Meyer, T. Pilati, D.M. Proserpio, G. Resnati, Chem. Eur. J. **13**, 5765 (2007)
7. M.D. Ward, Coord. Chem. Rev. **251**, 1663 (2007)
8. O.R. Evans, W.B. Lin, Acc. Chem. Res. **35**, 511 (2002)
9. S. Dibella, Chem. Soc. Rev. **30**, 355 (2001)
10. B.J. Coe, L.A. Jones, J.A. Harris et al., J. Am. Chem. Soc. **126**, 3880 (2004)
11. N. Yasuda, Y. Hsiao, M.S. Jensen, N.R. Rivera, C. Yang, K.M. Wells, Y.J. James, M. Palucki, L. Tan, P.G. Dormer, R.P. Volante, D.L. Hughes, P.J. Reider, J. Org. Chem. **69**, 1959 (2004)
12. M.C. Wani, P.E. Ronman, J.T. Lindley, M.E. Wall, J. Med. Chem. **23**, 554 (1980)
13. J.A. Wendt, S.D. Deeter, S.E. Bove, C.S. Knauer, R.M. Brooker, C.A. Szafran, R.D. Schwarz, J.J. Kinsorac, K.S. Kilgorec, Bioorg. Med. Chem. Lett. **17**, 5396 (2007)
14. T.G. Majewicz, P. Caluwe, J. Org. Chem. **40**(23), 3407 (1975)

15. G.L. Eichhorn, R.A. Latif, J. Am. Chem. Soc. **76**, 5180 (1954)
16. Q. Jingui, S. Nanbing, D. Chaoyang, Y. Chuluo, L. Daoyu, W.D. Michael, W. Baichang, C. Chuangtian, Polyhedron **18**, 3461 (1999)
17. Y. Li, Z. Leu, H. Deng, Acta Crystallogr. Sect. E: Struct. Rep. Online **E63**, m3065 (2007)
18. C.C. Fernández, L.M. Thomson, J.G. Mascarós, X. Ouyang, K.R. Dunbar, Inorg. Chem. **41**, 1523 (2002)
19. K.S. Hagen, Inorg. Chem. **39**, 5867 (2000)
20. Vogel's *Text Book of Practical Organic Chemistry*, (Revised by B.S. Furniss, A.J. Hannaford, P.W.G. Smith, A.R. Tatchell), 5th (U. K.), Edn. Longmann (ELBS): Essex (U.K), (1991)
21. D.D. Perrin, W.F. Armarego, D.R. Perrin, *Purification of laboratory Chemicals* (Pergamon, Oxford, 1986)
22. Bruker Analytical X-ray systems. SAINT – Ver. 6.45 copyright (c), Inc Madison, Wisconsin, USA, (2003)
23. G.M. Sheldrick, SADABS *Program for Absorption Correction,* (version 2.10); Analytical X—ray systems, Madison, Wisconsin, USA, (2003)
24. G.M. Sheldrick, *SHELXL–97, A Program for crystal structures Refinement* (University of Göttingen, Germany, 1997)
25. M.S. Blois, Nature. **181**, 1199 (1958)
26. P. Shekan, R. Storeng, D. Scudiero, A. Monks, J. Mc Mohan, D. Vistica, J.T. Warren, H. Bokesch, S. Kenncy, M.R. Boyd, Natl. Cancer. Inst. **82**, 1107 (1990)
27. A. Monks, D. Scudiero, P. Skehan, R. Shoemaker, K. Paull, D. Vistica, C. Hose, J. Langley, P. Cronise, A. Vaigro-Wolff, M. Gray-Goodrich, H. Campbell, J. Mayo, M.J. Boyd, Natl. Cancer Inst. **83**, 757 (1991)
28. K. Nakamoto, *Infrared and Raman spectra of Inorganic and Coordination compounds*, 5th edn. (Wiley-Interscience, New York, 1997)
29. M. Sandstrom, I. Persson, Acta Chem. Scand. **44**, 653 (1990)
30. S. Sobha, R. Mahalakshmi, N. Raman, Spectrochim. Acta **92**, 175 (2012)
31. D.M.A. El–Aziz, S.E.H. Etaiw, E.A. Ali, J. Mol. Struct. **1048**, 487 (2012)
32. Y. Li, Z.Y. Yang, J. Fluoresc. **20**, 329 (2010)
33. S.E.H. Etaiw, D.M.A. El–Aziz, E.H.A. El–Zaher, E.A. Ali, Spectrochim. Acta **79**, 1331 (2011)
34. D. Banerjea, *Coordination Chemistry* (Tata McGraw–Hill Publisher, London, 1993)
35. R.S. Joseyphus, M.S. Nair, Arabian J. Chem. **3**, 195 (2010)
36. V.K. Naveen, S.K. Gurunath, B. Srinivasa, K. Vidyanand, K.J. Revankar, J. Coord. Chem. **63**, 3301 (2010)
37. O.A.M. Ali, Spectrochim. Acta A **132**, 52 (2014)
38. D. Arish, M. Sivankaran Nair, J. Mol. Struct. **983**, 112 (2010)
39. D. Kivelson, R. Nieman, J. Chem Phys. **35**(1), 149 (1961)
40. B.J. Hathaway, D.E. Billing, Coord. Chem. Rev. **5**, 143 (1970)
41. B.J. Hathaway, Struct. Bond. (Berlin) **57**, 55 (1984)
42. B. Roopashree, V. Gayatri, H. Mukund, J. Coord. Chem. **65**, 1354 (2012)
43. J. Baldwin, C. Chothia, J. Mol. Biol. **129**, 175 (1979)
44. W.J. Pietro, M.M. Francl, W.J. Hehre, D.J. Defrees, J.A. Pople, J.S. Binkley, J. Am. Chem. Soc. **104**, 5039 (1982)
45. M.J.N. Frisch, G.W. Trucks, H.B. Schlegel, *Gaussian 09, Revision B01* (Gaussian, Inc., Wallingford CT, 2009)
46. V. Kumar, A. Abbas, J. Aster, *Robbins basic pathology* (Elseviar, Saunders, Philadelphia, 2013)
47. T.J. Lynch, D.W. Bell, R. Sordella, S. Gurubhagavatula, R.A. Okimoto, B.W. Brannigan, P.L. Harris, S.M. Haserlat, J.G. Supko, F.G. Haluska, D.N. Louis, D.C. Christiani, J. Settleman, D.A. Haber, The New England Journal of Medicine **350**(21), 2129 (2004)